PAPER

Growth of twisted bilayer graphene through two-stage chemical vapor deposition

To cite this article: Che-Men Chu and Wei-Yen Woon 2020 *Nanotechnology* **31** 435603

IOP Publishing Nanotechnology

Nanotechnology **31** (2020) 435603 (10pp) https://doi.org/10.1088/1361-6528/aba39e

Growth of twisted bilayer graphene through two-stage chemical vapor deposition

Che-Men Chu and Wei-Yen Woon

Department of Physics, National Central University, Jungli 32054, Taiwan

E-mail: wywoon@phy.ncu.edu.tw

Received 18 May 2020, revised 29 June 2020
Accepted for publication 7 July 2020
Published 3 August 2020

Abstract

We investigate growth of twisted bilayer graphene through two-stage chemical vapor deposition (CVD). Exploiting the synergetic nucleation and growth dynamics involving carbon sources from the residual carbon impurities in Cu bulk and gaseous CH_x, sub-millimeter-sized single crystalline graphene grains with multiple merged adlayer grains formed underneath are grown on Cu substrate. The distribution of the twist angles is investigated through a computer algorithm utilizing spectral features from micro-Raman mapping. Besides the more thermodynamically stable AB-stacking (AB-BLG) or large angle (>15°) decoupled bilayer graphene (DC-BLG) configurations, there are some bilayer regions that contain specific twist angles (3–8°, 8–13°, and 11–15°) (termed as TBLG). The statistics show no TBLG formation for BLG with single nucleation center. The formation probability of TBLG is strongly dependent on the relative orientation of merging adlayer grains. Significant defects are found at the grain boundaries formed in AB-DC merging event without creating TBLG domain. The areal fraction of TBLG increases as H_2/CH_4 ratio increases. The growth mechanism of TBLG is discussed in light of the interactions between the second layer grains with consideration of strain generation during merging of adlayers.

Supplementary material for this article is available online

Keywords: twisted bilayer graphene, chemical vapor deposition, Raman spectroscopy

(Some figures may appear in colour only in the online journal)

1. Introduction

Since its discovery in 2004, graphene has been a hot research topic due to its unique electronic, mechanical, and thermal properties [1–3]. Chemical vapor deposition (CVD) involving hydrocarbon precursors and transition metal catalyst in a furnace system, is the most popular method for preparing high quality large scale graphene [4–6]. Scientifically, the nucleation and growth dynamics of graphene can serve as a good paradigm system for studying the physics of two dimensional film growth. It has been shown previously that the grain size, nucleation density, and number of layers of CVD grown graphene can be controlled through CH_4/H_2 ratio, temperature, total pressure, substrate treatment, and so on [7–14]. As a result, the electronic, optical, and mechanical properties of the graphene film can be tuned accordingly.

Bilayer graphene is an interesting material on its own. Bernal-stacked or AB-stacked bilayer graphene (AB-BLG) exhibits a tunable bandgap up to 250 meV when a transverse electric field is applied [15]. Therefore, the AB-BLG serves as a promising alternative material in potential electronics applications such as field-effect transistors [16, 17]. Nevertheless, growing a fully covered AB-BLG film is a challenging task because of significant differences in the carbon supply between the top first layer and the underneath adlayer, resulting in low areal ratio between the adlayer to first layer. Remarkable progress has been made recently in enlarging the coverage of the underneath adlayer. In particular, Yang *et al*

showed that by applying a growth and regrowth methodology in CVD process, the grain edge of the first layer would be H terminated, so that diffusion of carbon source underneath the top layer can be enhanced, and growth of the adlayer can be promoted significantly while the top layer growth is suppressed [18, 19]. The above work showed that manipulation of bilayer properties can be achieved through CVD by understanding the detailed nucleation and growth dynamics.

Very recently, breakthrough discoveries on the twisted bilayer graphene (TBLG) drew intensive attention from the research community. By stacking one graphene layer on top of another at a relative twist angle θ, an artificial TBLG can be formed. The stacking of two graphene layers results in a Moir´e pattern superlattice potential. It was observed that TBLG exhibits unconventional insulator and superconductor phases near the magic angle $\theta = 1.05°$ [20, 21]. Since then, many studies have been devoted to understanding the insulator and superconductor phases of the TBLG [22]. Nevertheless, the conventional TBLG fabrication methodologies are difficult to be up-scaled for mass production.

Raman spectroscopy has been the primary experimental tool for analyzing the vibrational properties of both AB-BLG graphene or TBLG [23–25]. A resonant enhancement of G band and an additional R band have been found at a critical angle θc when the incident laser energy is equal to the gap between the electron and hole van-Hove singularities [26, 27]. Furthermore, the position, width, and intensity of the 2D peaks has been found to be function of twist angle, with an angle dependence on the electronic structure and the van-Hove singularities [28–31]. An additional R' side-band appears beside the G band at $\theta = 3–8°$. Altogether, the above signatures can be used to unambiguously distinguish the twist angle of the bilayer graphene into several different categories. In this work, by employing the previously attained knowledge, we develop a micro-Raman mapping methodology equipped with an algorithm to achieve areal identification of the TBLG grown through CVD.

In our previous work [32], we found that uniform millimeter or submillimeter-sized single crystalline graphene grains can be formed under growth conditions with high temperature and high hydrogen to methane ratio. Moreover, in each first layered grain, we found numerous multi-layered adlayer grains with wide size distribution. It was found that the twist angle θ of each bilayer grain can be different even in the same single crystalline first layer grain. However, it was not clear what role does the residual carbon plays in the development of the adlayer growth and what will happen if the adlayer grains merge and interact. In this work, through a unique second growth approach, we clarify the role played by the residual carbon in the development of the adlayer growth and its impact to the TBLG growth. We conduct statistical investigation on the areal θ distribution of TBLG and relate it to interactions between the adlayer grains by carefully looking into the Raman features around the TBLG grains. Compared to previous works in which Raman mapping of TBLG was conducted on CVD grown graphene to investigate the special features in Raman spectroscopy that could give more information to the physical interactions between layers, our focus is to investigate the origin of formation of TBLG through grain-grain interactions. Furthermore, we related the formation of twist bilayer graphene to the CVD growth conditions. Demonstration on the controllability of TBLG areal ratio is also presented. Finally, we present a phenomelogical model of the TBLG growth based on the above observation.

2. Experiment section

2.1. Growth of multilayered graphene

The setup of the tool used in this work is similar to our previous work, and the details can be found therein [33]. In brief, a pretreated (polished and cleaned) Cu foil was placed on a SiC boat for thermal processing in a cold-wall rapid thermal apparatus (As-Micro RTP System, ANNEALSYS). The major thermal process for CVD graphene growth includes four stages: A ramping (10 min) to target temperature, a constant temperature period at 1000 °C for 30 min under a common gas ratio (details in following) to allow for preferred form of multilayer growth, and another 30 min (incomplete) or 1 h (fully covered) of growth under various gas ratio in order to tune the areal proportion of multilayer grains, followed by a cooling to room temperature for 15 min. During stage 1, The copper substrate was mildly oxidized by exposure to hot Ar (500 sccm, 960 mtorr) that contains low concentration of residual oxygen. After the ramping period, graphene film was grown with CVD involving H_2/CH_4 ratio = 30:1 for 30 min so that there are usually more than one small multilayered grains under a single layer graphene grain while the front and back-sides of the Cu substrate are not fully covered by graphene. After that, various gas mixtures with H_2/CH_4 ratio from 20:1 to 40:1 ($H_2 = 20\sim40$ sccm, $CH_4 = 1$ sccm) are injected into the chamber to allow for various form of grain-grain interactions between the bilayer grains. For the above steps, the chamber pressure (1.4 torr) is maintained by the accompanying Ar flow. After graphene growth, a fast cooling (cooled down to below 800 °C within 1 min) is applied by switching off the heating lamp with continuous Ar, H_2 and CH_4 flows until cooling down to room temperature within 15 min.

2.2. Methods and data analysis

The CVD grown graphene is first examined under scanning electron microscope (SEM) with low operating voltage at 10 KV (Jeol JSM7000F). Compared to the single layered counterpart, the multi-layered regions appear to be darker because part of the secondary electrons are blocked. Although the multi-layered graphene grains can be unambiguously identified in SEM, the twist angles between the layers are not distinguishable. In order to identify the twist angle distribution, some of the graphene sheets are transferred to silicon substrate buffered with 300 nm SiO_2 using a bubble free transfer method [34]. Subsequently, the samples were examined under optical microscopy (OM) (BX51, Olympus) to identify the number of layer by color contrast, and located for micro-Raman measurement. In each transferred sample, there are 50–100 grains that contain multiple adlayer grains that merge, and

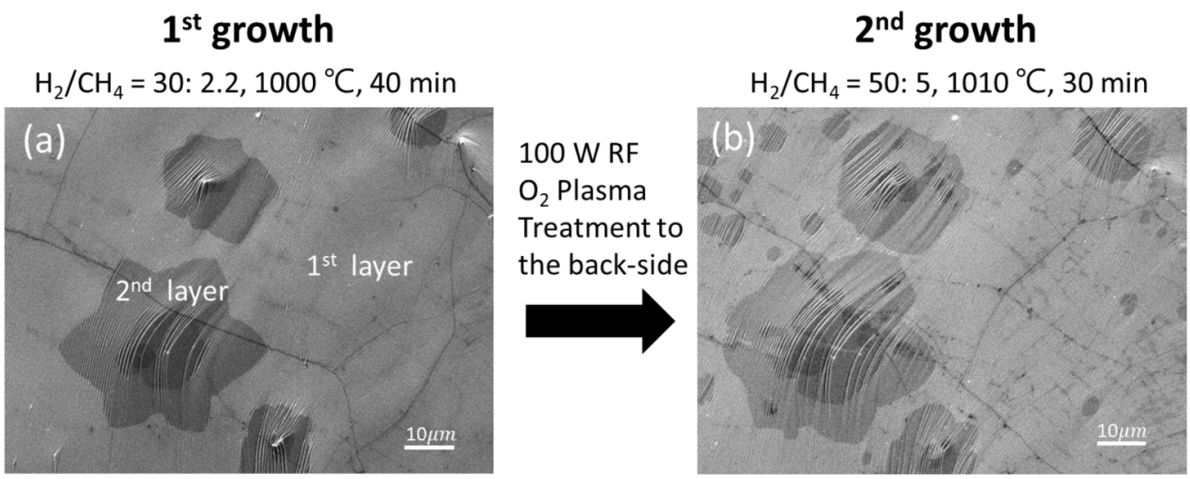

Figure 1. SEM image of the front-side of graphene covered Cu for (a) first growth for 40 min under condition of H_2/CH_4 ratio = 30:2.2 at 1000 °C, (b) second growth for 30 min under condition of H_2/CH_4 ratio = 50:5 at 1010 °C, after 7 min of O_2 plasma treatment at RF power = 100 W to the back-side of Cu to completely etch away the single layer graphene.

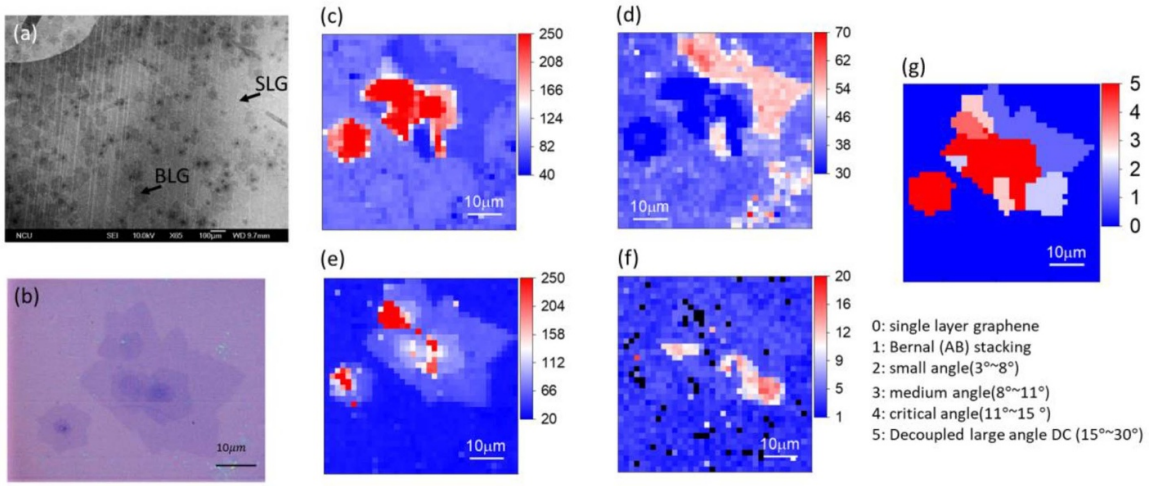

Figure 2. (a) Typical SEM image of a fully covered multi-layered graphene sheet. (b) Zoom-in OM image of graphene film grown under H_2/CH_4 ratio = 40:1 condition. Corresponding Raman mapping showing (c) intensity of 2D peak, (d) FWHM of 2D peak, (e) intensity of G peak and (f) intensity of R' peak. (g) the corresponding twist angle distribution.

we perform Raman mapping for each of them. The morphology and twist angle θ distribution of the as-grown graphene under each CVD condition is highly reproducible, and we have conducted three runs for each CVD conditions for the data collection. Altogether, for all CVD conditions, we can collect more than 100 events for grain-grain interactions of different types, excluding the areas where contaminants and defects interfering the judgement. The acquired OM and Raman mapping images were processed and analyzed with a home built Labview algorithm to reveal the twist angle of each area. We present the work flow of the algorithm in figure S1 (available online at stacks.iop.org/NANO/31/435603/mmedia) . First, by color contrast, the number of layer can be identified, and the analysis is focused on the BLG part. Second, a threshold at wavenumber = 1615 cm^{-1} is set to filter the R' band. If the intensities of R' band in an area exceed the threshold, θ in such area is then identified as 3–8°(the first spectrum from top shown in figure S2). Subsequently, for area outside of the above marked region, the symmetry and width of 2D band, along with the intensity of the G band, are examined. For area with highly asymmetric 2D band with full width at half maximum (FWHM) larger than 40 cm^{-1}, it is marked as AB-BLG (figure S2, second spectrum from top). Note that the twist angle θ may not necessarily be zero because the above Raman feature holds for $0° < \theta < 3°$. While for area with highly symmetric and narrow 2D band (FWHM < 30 cm^{-1}), it is identified as decoupled bilayer graphene (DC-BLG) (figure S2, third spectrum from top). In our case the twist angle θ for DC-BLG can be spanned from >15°up to <30° (most probably close to 30° since it is far from van-Hove singularity) On the other hand, for area with significantly high G band than the single layer graphene (SLG) ($I_G/I_{G(SLG)} > 3$) and having a R band intensity (1460 cm^{-1}) higher than the threshold value, the twist angle is then marked as the critical angle (van-Hove singularity) θc = 11–15° (figure S2, second spectrum from bottom). Last, the leftover areas with symmetric 2D band and

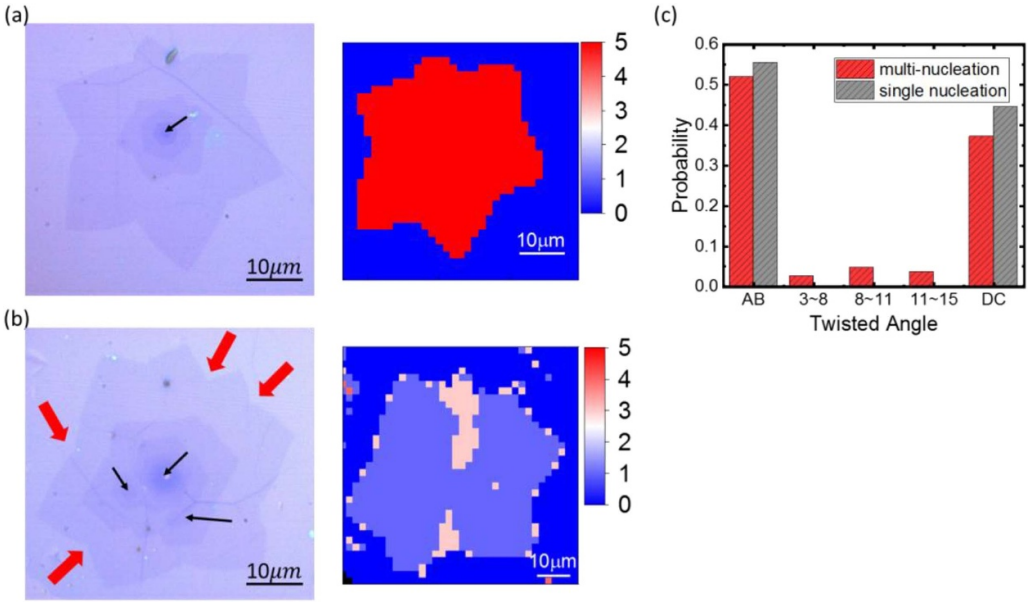

Figure 3. OM image and Raman mapping of MLG grain with (a) single nucleation center, (b) multiple nucleation centers. Black arrows indicate the nucleation centers. Bold red arrows indicate the growth fronts which are relatively slower. (c) Probability of TBLG generation in multi-nucleation and single nucleation MLG.

G band intensity slightly higher than the G band intensity of SLG ($I_G/I_{G(SLG)}$ ~1.2) is then assigned as having $\theta = 8$–$11°$ (figure S2, the bottom-most spectrum). Consequently, six categories of twist angle θ can be identified and marked with color scales. We term $\theta = 3$–$8°$, 8–11°, 11–15° as small angle, intermediate angle, and critical angle, respectively. Altogether, to simplify further analysis, the above BLG areas are further grouped as TBLG, in contrast to the more thermodynamically favored AB-BLG and DC-BLG. For the areas with more than two layer of graphene, the twist angle is only considered for BLG through assumption of the continuity of grain orientation.

3. Result and discussion

First we clarify the origin of the carbon sources for the growth of multiple adlayers underneath the first layer graphene. It is perceived that during growth process, the out-diffused carbon sources from the Cu bulk can become nucleation centers for adlayer grains underneath the first layer. Meanwhile, before the first layer graphene fully covers the Cu surface, carbon sources can diffuse under the first layer graphene grain to enable growth of adlayer grain if the edges of the first layer graphene grain are not tightly pinned to the Cu surface (i.e. H-terminated for instance). However, if the first layer is fully covered at one point of the growth process, can the carbon sources inside the bulk contribute to the further growth of the adlayer until they merge and interact? To check the above, we first grow fully covered graphene on Cu with a H_2/CH_4 ratio of 30:2.2 at 1000 °C for 40 min. Due to asymmetry of carbon supply between the front and back-side surfaces of the Cu substrate, the back-side Cu surface is fully covered by purely single layer while the front-side contains some small second layer grains underneath the fully covered first layer graphene (figure 2(a)). As the front-side and back-side of the Cu surface is fully covered by graphene film, further prolonged growth process does not change the morphology of the adlayer grains under the continuous first layer because there is no pathway for the carbon sources to be introduced into (images not shown). The above observation indicate that the carbon flux coming directly through the defects in the fully covered graphene or grain boundaries are comparably insignificant within the CVD growth time. We then employed a seven-minute O_2 plasma treatment (RF power 100 W) to the back-side of Cu substrate (with the front-side sealed to prevent plasma etching) to completely etch away the graphene film on the back-side of Cu substrate (verified by SEM). Subsequently, the sample was put back into the CVD chamber for second CVD growth (H_2/CH_4 ratio of 50:5 at 1010 °C for 30 min). Figure 1(b) shows the SEM image of graphene film acquired at the same location of the sample after the second growth process. The overall growth rate of the second layer is lower than the run shown in figure 1(a) because the major carbon diffusion pathway from the edge of first layer is no longer available. It is clear that while the existing adlayer grains increased in size, there are also new adlayer grains appear sporadically (preferably at defects sites such as grain boundaries and wrinkles), with different sizes (i.e. the nucleation started at different time). Since the above experiment excluded contribution from the carbon sources from gaseous CH_x diffusing underneath first layer directly through the edges of the first layer, the above observation proved that carbon precipitation from Cu bulk can both contribute to nucleation center formation and grain size growth. Second, the newly appeared adlayer grains can 'get in the way' of the growth front propagation of existing adlayer grains if the carbon sources are further supplied, judging from the SEM image. In such situation, it is expected that grain

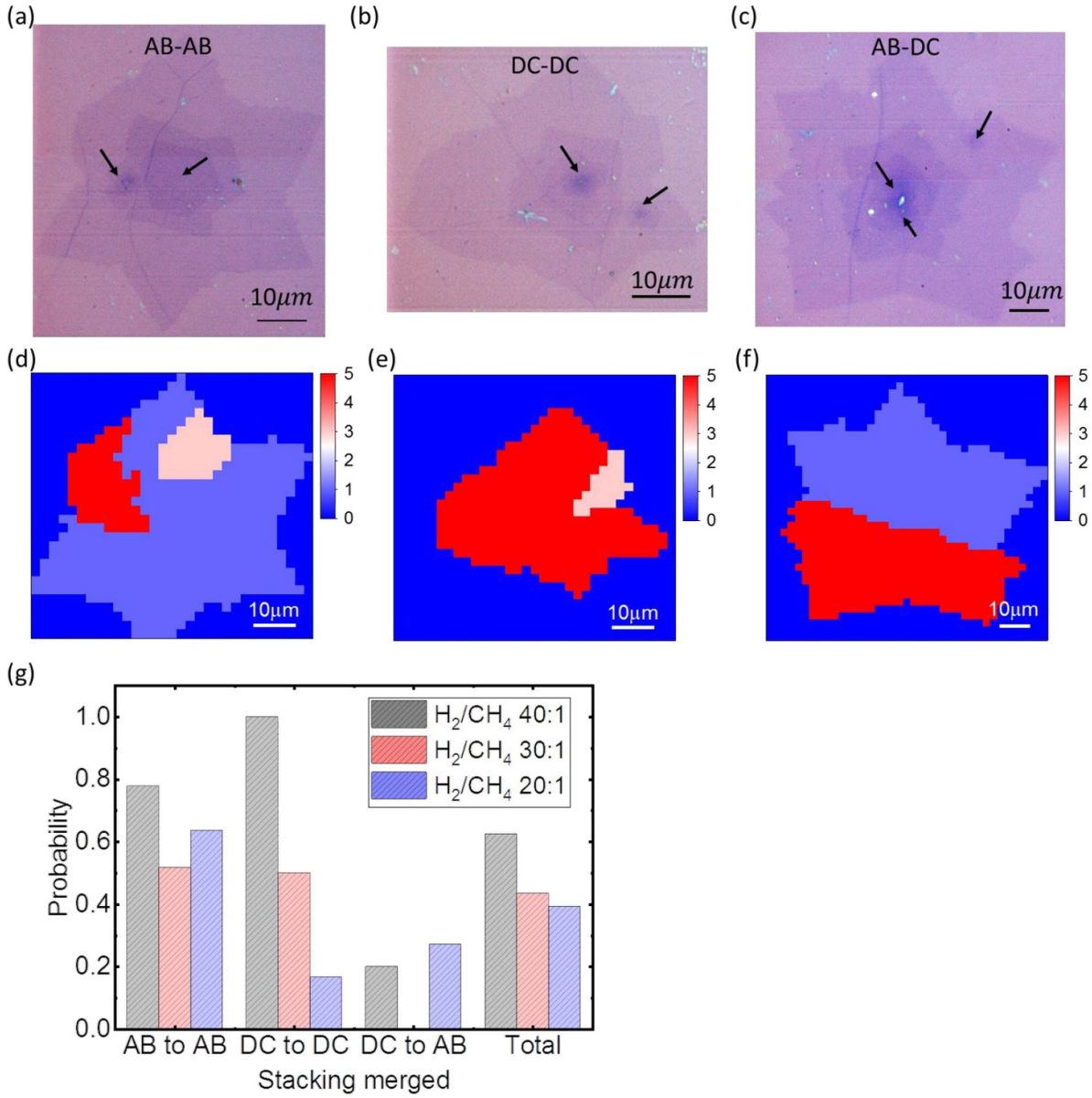

Figure 4. OM image and Raman mapping of TBLG generated through merging of (a), (d) AB-AB, (b), (e) DC-DC, and (c), (f) AB-DC (g) probability of TBLG formation through merging of BLG with various relative orientations.

boundaries can be formed between the adlayers if the merging grains have different orientation angles, and result in formation of polycrystalline adlayer grains underneath the single domain crystalline first layer, similar to the polycrystalline formation mechanism of single layer graphene [35]. The understanding on the role played by the carbon sources in the Cu bulk and the possibilities of merging between adlayer grains with different orientations are vital for understanding the interaction between adlayer grains and the formation of TBLG, as we will discuss in later part of this paper.

Figure 2(a) shows the SEM image of a fully covered multilayered graphene sheet grown on Cu under second growth condition at H_2/CH_4 ratio = 40:1. Figure 2(b) shows the typical OM image of a BLG region with various Raman features. The corresponding Raman mapping images are shown in figures 2(c)–(f). The intensity and FWHM of 2D band are plotted as color map in figures 2(c) and (d), respectively. The intensity of G band is plotted in figure 2(e), while the intensities of R' band is plotted in figure 2(f). The map of R band is relatively difficult to show due to poorer contrast, but can be identified with careful inspection of the spectrum (shown in the spectra in figure S2). Combining the above information and analyses through the computer algorithm, we can unambiguously map the twist angle distribution in the above mentioned area, as shown in figure 2(g).

More careful inspection of the Raman mapping shows that BLG can be formed by stacking of first layer grain with either an isolated adlayer (figure 3(a)) or closely located adlayer grains underneath (figure 3(b)). An also noteworthy point is that the TBLG areas usually span from the edge of the adlayer, where the growth front is indented inward (the red arrows indicated in the figure 3(b)), i.e. where the growth rate of the

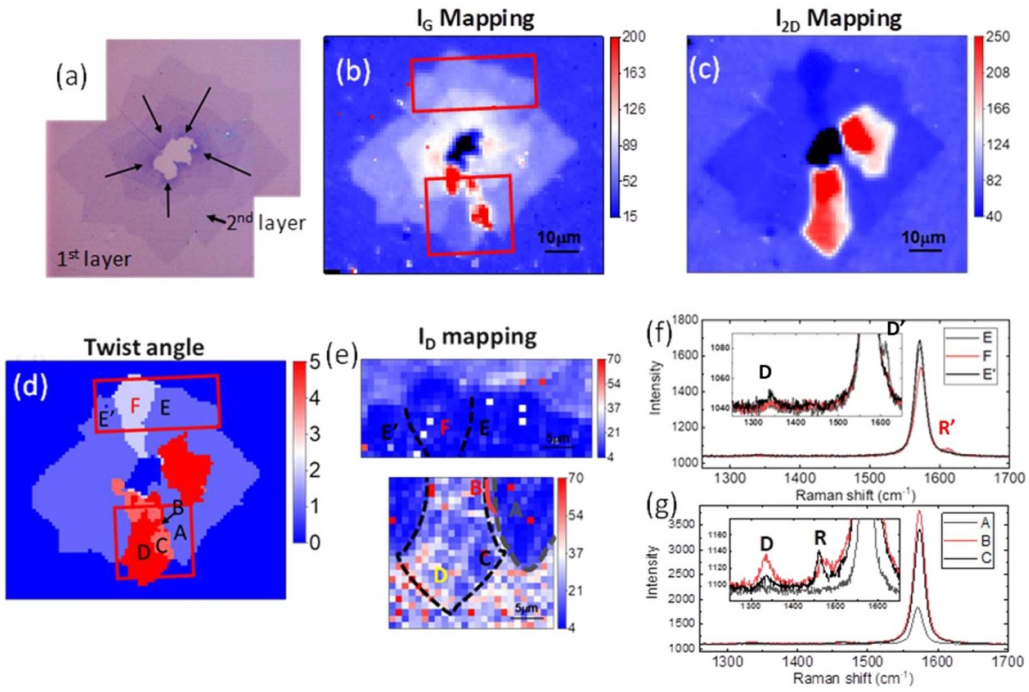

Figure 5. (a) OM image of a five-nucleation center adlayer, and the corresponding (b) I_G mapping, (c) I_{2D} mapping, and (d) twist angle mapping. (e) The zoom-in views of ID mapping for two regions of interest encircled in (d). (f) The corresponding Raman spectra acquired at locations indicated in the (f) upper and (g) bottom part of the BLG. Insets in figures show the close-up view of the spectra around D and R peak positions.

adlayer is relatively lower (or there exist a 'younger' adlayer grain that appear later in the growth process). Interestingly, through Raman mapping of more than 100 grains, we find that there is no TBLG for the isolated adlayer (single nucleation center), i.e. the isolated BLG is either AB-BLG or DC-BLG. The probability of AB-BLG is slightly higher than the DC-BLG, but there is no TBLG founded. On the other hand, for the cases of multiple merged adlayers, we can find probability of TBLG formation in most cases (figure 3(c)). According to previous work [36], AB-BLG is the most stable configuration for BLG stacking, since it is energetically favored. DC-BLG, on the other hand, is the second most favorable configuration for BLG stacking since the two graphene layers are decoupled and they can be treated as two independent SLG stacked together. Our result above indicates that under the two stage-growth conditions employed in our experiment, the formation of TBLG is a *consequence of grain-grain interactions*, which is not energetically favored.

In light of the above observation, we further examine each grain-grain merging event to investigate if the propensity of TBLG formation depends on the relative orientation between the grains that merge together, namely AB-AB, DC-DC, and AB-DC, respectively. Figures 4(a)–(c) and (d)–(f), show the typical OM and Raman mapping for AB-AB, DC-DC, and AB-DC merging event under one large first layer grain, respectively. Figure 4(g) shows the probability of TBLG formation through merging of BLG with various twist angle configurations. It is clear that formation of TBLG is highly probable for DC-DC and AB-AB merging, but much less probable for AB-DC merging events. Furthermore, the dependence of TBLG formation on CVD condition are examined. Among them, for DC-DC case, the TBLG formation probability is highly dependent on the H_2/CH_4 ratio, in which the TBLG formation probability is significantly higher under H_2/CH_4 ratio = 40:1. On the other hand, for AB-AB case, the difference in TBLG formation probability is less sensitive to the H_2/CH_4 ratio, although it is still higher under H_2/CH_4 ratio = 40:1 condition. We find significantly low probability of TBLG formation for AB-DC cases, especially for H_2/CH_4 ratio = 30:1, where there is no TBLG formation event in the >100 events we have measured. The above observation suggests that not only does the hydrogen termination at grain edge play important role in TBLG formation, the coupling between first and adlayer, as well as the relative orientation between the merging/interacting grains, also play important roles in TBLG formation.3

Further exploration into the Raman mapping of a particular multi-adlayer merging event helps to clarify the origin of TBLG formation in adlayer grains merging event. As shown in figure 5(a), the OM image shows that there are five nucleation centers located closely to each other, as indicated by the black arrows. The transferred multi-layered graphene is easily broken at the multi-nucleation site due to existence of impurities (hence the reason for favorable nucleation). Nevertheless, through Raman mapping, we can still unambiguously identify the twist angles of each adlayer domain through detailed classification by the Raman features, as exemplified by the G and 2D band intensity mapping shown in figures 5(b) and (c). Figure 5(d) shows the twist angle mapping. At the bottom part of the BLG domain, we can find a merging case of AB (right,

location A)—DC (left, location D) creates a wedge with critical angle (11–15°) TBLG (location C) and a boundary line with no TBLG created (i.e. $\theta > 15°$) (location B). On the other hand, in the upper part, there is a AB-AB merging event, and we can find a narrow wedge of small angle (3–8°) TBLG domain (location F) sandwiched between the two AB-BLGs (location E and E'). The D band intensity mappings of the above two cases are shown in figure 5(e). While there is an additional distinctive R' band found at the small angle TBLG (3–8°) domain (inset of figure 5(f)), there is no D band found at the boundaries between AB BLGs and the small angle TBLG, as shown in figure 5(f). On the other hand, it is clear that there is no detectable D band in the AB-BLG (locations A). However, clear D band can be found at the boundary between AB and DC BLGs (locations B and C). The D band intensity at location B is significantly greater than location C. Moreover, the position of the R band at location B slightly blueshifts compared to the R band in location C (see inset in figure 5(g)). The above observations suggest that 5–7 dislocation defect line is created at the boundary between AB and DC BLGs. Overall speaking the above observations support the phenomelogical model we propose.

We are not able to observe the exact dynamics of the TBLG formation during the CVD process due to limitation in instrumentation. Here we present a phenomenological model based on the above observations, as illustrated in figure 6. The validity of this model needs to be further proved through more detailed characterization, Therefore we have to stress that the phenomelogical model are speculative and remains as a proposal for experiment for the next stage. Nevertheless, the reason we present it here is to encourage input from the theoretical calculation and simulation. In short, nucleation of first-layer graphene starts at the surface defect or carbon supersaturation site. The grain keeps growing through addition of carbon atoms within the grain's capture radius. For a first layer with H-terminated grain edge, the carbon sources diffuse on the copper surface can either add to the first layer and lead to its growth or diffuse underneath the first layer and lead to the growth of adlayers at the existing or newly formed nucleation sites. Due to suppressed sublimation of adlayer grains by the capping of first layer, the small adlayer grains survive and grow, unlike those exposed on catalyst surface. The number of adlayer grains increases through continuous nucleation from the catalyst substrate. The stacking between the first layer and adlayer is energetically determined, i.e. formation of AB-BLG or DC-BLG are favored. The adlayer grains grow through attachment of carbon sources diffused underneath the first layer grain and can merge with each other to form larger grain. During merging, strain is developed due to mismatch of grain orientation. The strength of strain is related to the form of grain boundaries generated, and they are dependent on the misorientation angle between the merging grains. In particular, from previous work [37], it is found that when two single layer graphene grains merge, strain cancellation can occur around the (5, 7) pairs for misorientation angle $\varphi = (21.79°, 42.1°)$, while for other misorientation angles, asymmetric and disconnected grain boundary can occur and results in strain. On the other hand, in other previous works [35, 38], it was revealed that merging of more than one grains of single layer graphene during growth would result in generation of grain boundary between the misoriented grains because the graphene growth rate along the armchair (AC) edge on Cu is faster than that of the zig-zag (ZZ) edge on Cu. The distribution of the misorientation angle is widely spread, with higher probability around 30 degree. The previous experiment was conducted under high temperature (1070 °C–1100 °C, liquid Cu condition), so it is expected that the grains are free to rotate to the more energetically favored orientation when subject to strain. Therefore, they observe no generation of grain area with orientation different from the original orientation of the grains that merge together. In our case, with the additional coupling between first and second layer, and the lower temperature used (solid Cu), the strain generated when two grains merge cannot be easily relaxed through large scale reorientation, as in the case of CVD on liquid Cu. Therefore, we expect that there will be local relaxation of strain through generation of small wedges with different orientations. In our case, the fast-grown single crystalline large area first layer preexists before the growth of adlayers underneath. The above discussed merging of the adlayers, and the corresponding generation of wedges with different orientation angles would result in TBLG domains when considering the stacking with the top first-layer. In our model, the strength of strain, as well as the constraint set by the coupling from the preexisting first layer, determines if the reorientation of grain (generation of the non-energetically favored TBLG domains) could occur. Following the above idea, it is thought that the misorientation angle between AB-BLG (0–3°) and DC-BLG (15–30°)falls between the range of $\varphi = (21.79°, 42.1°)$, less strain is generated, thus lower probability for TBLG generation. On the other hand, for the merging of more than two DC-BLGs, the twist angle between the first layer and the second layer underneath is in the range of >15°, and less than 30°. However, the relative misorientation angle between two DC-BLG can be between 0°to <60°, since we are not able to know the exact angle and the direction each individual grain through Raman spectroscopy as the fingerprints of the spectra only shows dependence within a range of twist angle. Therefore, the merging of more than two DC-BLGs would be a mixed case of with or without strain generation. As a result, the probability for generation of TBLG wedge would be higher than the case for AB-DC merging events. As for the merging of more than two AB-stacked adlayers, it appears impossible to result in TBLG formation in first glance. However, considering the fact that the Raman characterization only allow us to limit the twist angle of the AB-BLG to <3°, thus the relative misorientation angle between two AB-BLG can be between 0 and 6°. Therefore, the merging of so-called AB-BLG grains would result in strain if it is not perfectly zero twist angle, and can give rise to wedges with different orientation, mainly with small twist angle <8°, with strain relaxation through generation of accompanying connected 5–7 defects along the grain boundaries. Furthermore, the growth fronts of adlayer with more H-termination grow slower and is less strongly coupled to both

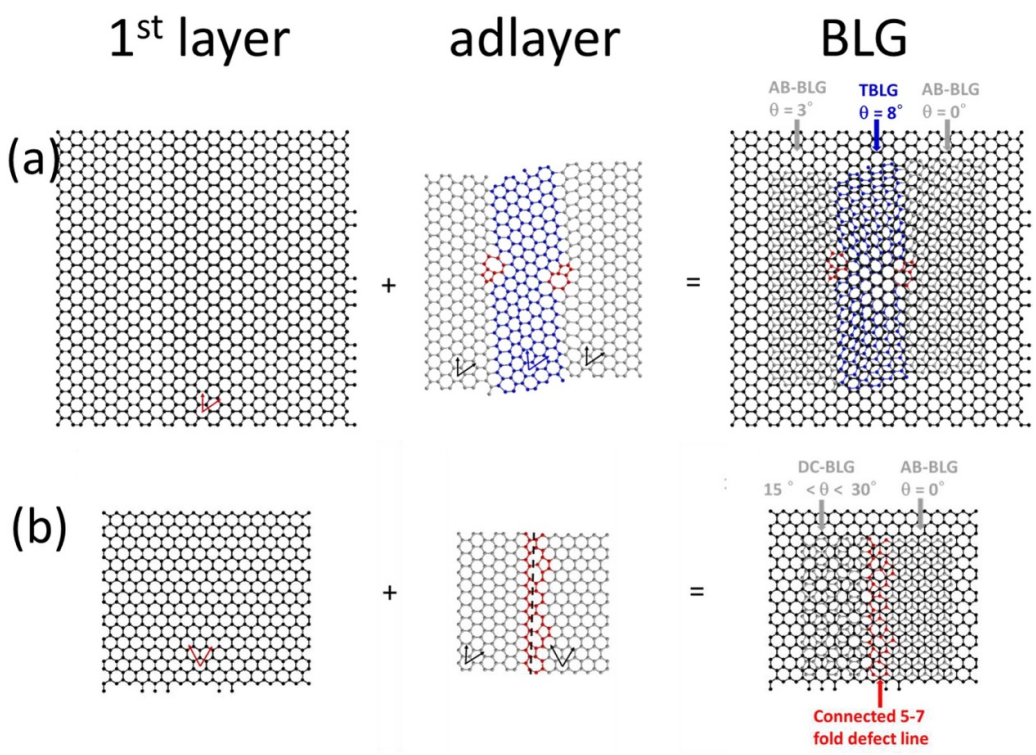

Figure 6. Merging event of (a) AB-AB BLGs creates a wedge of small angle TBLG between the two AB-BLG adlayers while the 5–7 defect density is low, (b) AB-DC BLGs creates continuous 5–7 defect line along the boundary and relax strain due to misorientation but creates no TBLG domain between the two merging adlayer grains.

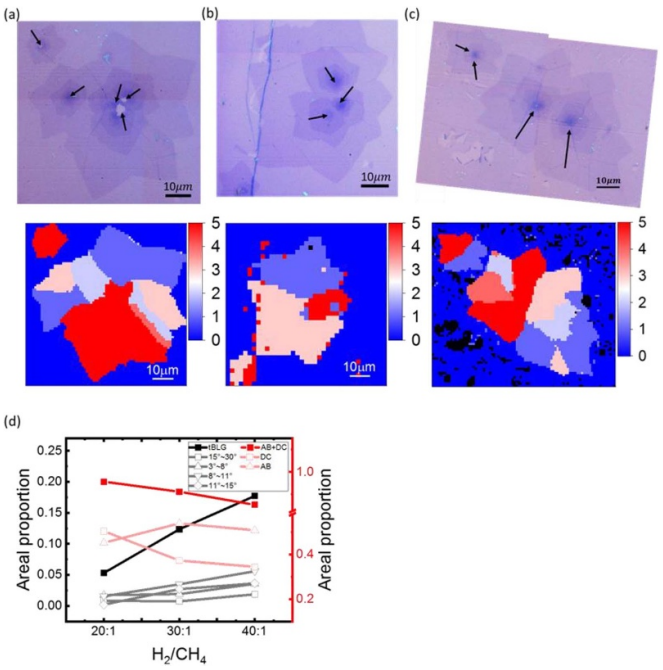

Figure 7. Typical OM image and Raman mapping of fully covered graphene film grown under H_2/CH_4 ratio of (a) 20:1, (b) 30:1, and (c) 40:1, respectively. The black arrows indicate nucleation centers. (d) Areal proportion of BLG with different twist angle versus H_2/CH_4 ratio.

the copper surface or the first layer. Therefore, the reorientation of growth direction (generation of wedges with different orientation angle) could occur at the growth fronts with more abundant H termination. According to above scenarios, it is expected that under higher H_2/CH_4 condition, H termination at the first layer could also promotes the carbon diffusion underneath and enhances the probability of inter-adlayer interaction since the distance between the growth fronts of

adlayer grains is effectively shortened (as adlayer grain size grows).

In light of the above proposed model, we further examine the effect of H_2/CH_4 ratio on the areal proportion of BLG with specific twist angle relative to the overall BLG area in a fully covered graphene film. Figures 7(a)–(c) show the typical optical images and Raman mapping of graphene grains grown under different H_2/CH_4 ratio, respectively. It is clear that the areal proportion of DC-BLG and AB-BLG is greater under H_2/CH_4 ratio = 20:1, while the areal proportion of TBLG increases significantly under H_2/CH_4 ratio = 40:1. Figure 7(d) shows the plot of areal proportion of each types of BLG versus H_2/CH_4 ratio. Overall speaking, as H_2/CH_4 ratio increases, the total areal proportion of TBLG increases, while the areal proportion of AB-BLG and DC-BLG decrease. The above observation indicates the possibility to produce TBLG with controllable manner. It is noteworthy to consider the effect of strain generated before or after the transfer process on the width of defect lines between adlayers since thre presence of such defect lines may impact the atomic arrangement of the incorporated carbon atoms around the grain boundaries. The above issue would be further investigated in the future work. Furthermore, we expect that the magic angle TBLG may be located around the boundaries between AB-BLG and the strain generated TBLG. However, the identification of such areas may need more delicate tools such as micro-low energy electron diffraction, nanometer resolution angle resolved photoelectron spectroscopy (ongoing) or high resolution scanning tunneling microscopy, and is currently out of the scope of this paper.

4. Conclusion

In conclusion, we investigate the growth of TBLG through a two-stage CVD. It is concluded that carbon sources precipitated from the Cu bulk can contribute both to the nucleation and growth of adlayer grains underneath a single crystalline first-layer graphene grain. Detailed exploration of Raman features reveal rich information on the grain-grain interactions underneath the first layer grain. Under the growth conditions employed, we found that the formation of TBLG is a result from inter-adlayer interactions. Furthermore, the probability of TBLG formation depends strongly on the relative orientations of the interacting adlayer grains. The H_2/CH_4 ratio can strongly affect the areal proportion of TBLG/BLG in a fully grown graphene film. Overall, a phenomenological model for the growth mechanism of the TBLG is presented in light of the interactions between the adlayer grains.

Acknowledgments

This work is supported by the Ministry of Science and Technology of Taiwan under contract MOST 106-2112-M008-003-MY3 and MOST-109-2628-M-008-004-MY3.

ORCID iDs

Che-Men Chu https://orcid.org/0000-0002-0350-287X
Wei-Yen Woon https://orcid.org/0000-0001-7299-9122

References

[1] Castro Neto A H, Guinea F, Peres N M R, Novoselov K S and Geim A K 2009 The electronic properties of graphene *Rev. Mod. Phys.* **81** 109–62
[2] Novoselov K S, Geim A K, Morozov S V, Jiang D, Zhang Y Dubonos S V Grigorieva I V and Firsov A A 2004 Electric field effect in atomically thin carbon films *Science* **306** 666–9
[3] Balandin A A, Ghosh S, Bao W, Calizo I, Teweldebrhan D, Miao F and Lau C N 2008 Superior thermal conductivity of single-layer graphene *Nano Lett.* **8** 902–7
[4] Geim A K and Novoselov K S 2007 The rise of graphene *Nat. Mater.* **6** 183–91
[5] Li X *et al* 2009 Large-area synthesis of high-quality and uniform graphene films on copper foils *Science* **324** 1312–4
[6] Li X *et al* 2010 Graphene films with large domain size by a two-step chemical vapor deposition process *Nano Lett.* **10** 4328–34
[7] Li X, Magnuson C W, Venugopal A, Tromp R M, Hannon J B, Vogel E M, Colombo L and Ruoff R S 2011 Large-area graphene single crystals grown by low-pressure chemical vapor deposition of methane on copper *J. Am. Chem. Soc.* **133** 2816–9
[8] Yu Q *et al* 2011 Control and characterization of individual grains and grain boundaries in graphene grown by chemical vapour deposition *Nat. Mater.* **10** 443–9
[9] Wang H, Wang G, Bao P, Yang S, Zhu W, Xie X and Zhang W-J 2012 Controllable synthesis of submillimeter single-crystal monolayer graphene domains on copper foils by suppressing nucleation *J. Am. Chem. Soc.* **134** 3627–30
[10] Li X, Colombo L and Ruoff R S 2016 Synthesis of graphene films on copper foils by chemical vapor deposition *Adv. Mater.* **28** 6247–52
[11] Chuang M C and Woon W Y 2016 Nucleation and growth dynamics of graphene on oxygen exposed copper substrate *Carbon* **103** 384–90
[12] Hao Y, Bharathi M S, Wang L, Liu Y, Chen H and Nie S 2013 The role of surface oxygen in the growth of large single-crystal graphene on copper *Science* **342** 720–3
[13] Choubak S, Levesque P L, Gaufres E, Biron M, Desjardins P and Martel R 2014 Graphene CVD: interplay between growth and etching on morphology and stacking by hydrogen and oxidizing impurities *J. Phys. Chem.* C **118** 21532–40
[14] Kotakoski J and Meyer J C 2012 Mechanical properties of polycrystalline graphene based on a realistic atomistic Model *Phys. Rev.* B **85** 195447
[15] Zhang Y, Tang -T-T, Girit C, Hao Z, Martin M C, Zettl A, Crommie M F, Shen Y R and Wang F 2009 Direct observation of a widely tunable bandgap in bilayer graphene *Nature* **459** 820–3
[16] Xia F, Farmer D B, Lin Y M and Avouris P 2010 Graphene field-effect transistors with high on/off current ratio and large transport band gap at room temperature *Nano Lett.* **10** 715–8
[17] Schwierz F 2010 Graphene transistors *Nat. Nanotechnol.* **5** 487–96
[18] Yang N, Choi K, Robertson J and Park H G 2017 Layer-selective synthesis of bilayer graphene via chemical vapor deposition *2D Mater.* **4** 035023
[19] Vlassiouk I, Regmi M, Fulvio P, Dai S, Datskos P, Eres G and Smirnov S 2011 Role of hydrogen in chemical vapor

deposition growth of large single-crystal graphene *ACS Nano* **5** 6069–76
[20] Cao Y, Fatemi V, Fang S, Watanabe K, Taniguchi T, Kaxiras E and Jarillo-Herrero P 2018 Unconventional superconductivity in magic-angle graphene superlattices *Nature* **556** 43–50
[21] Cao Y, Fatemi V, Tomarken S L, Luo J Y and Sanchez-Yamagishi J D 2018 Correlated insulator behaviour at half-filling in magic-angle graphene superlattices *Nature* **556** 80–84
[22] González J and Stauber T 2019 Kohn-Luttinger Superconductivity in twisted bilayer graphene *Phys. Rev. Lett.* **122** 026801
[23] Lui C H, Malard L M, Kim S, Lantz G, Laverge F E, Saito R and Heinz T F 2012 Observation of layer-breathing mode vibrations in few-layer graphene through combination Raman scattering *Nano Lett.* **12** 5539–44
[24] He R, Chung T-F, Delaney C, Keiser C, Jauregui L A, Shand P M, Chancey C C, Wang Y, Bao J and Chen Y P 2013 Observation of low energy Raman modes in twisted bilayer graphene *Nano Lett.* **13** 3594–601
[25] Havener R W, Zhuang H, Brown L, Hennig R G and Park J 2012 Angle-resolved Raman imaging of interlayer rotations and interactions in twisted bilayer graphene *Nano Lett.* **12** 3162–7
[26] Ni Z, Liu L, Wang Y, Zheng Z, Li L-J, Ting Y and Shen Z 2009 G-band Raman double resonance in twisted bilayer graphene: evidence of band splitting and folding *Phys. Rev.* B **80** 125404
[27] Kim K, Coh S, Tan L Z, Regan W, Yuk J M, Chatterjee E, Crommie M F, Cohen M L, Louie S G and Zettl A 2012 Raman spectroscopy study of rotated double-layer graphene: misorientation-angle dependence of electronic structure *Phys. Rev. Lett.* **108** 246103
[28] Brown L, Hovden R, Huang P, Wojcik M, Muller D A and Park J 2012 Twinning and twisting of tri- and bilayer graphene *Nano Lett.* **12** 1609–15
[29] Park K-D, Raschke M B, Atkin J M, Lee Y H and Jeong M S 2017 Probing bilayer grain boundaries in large-area graphene with tip-enhanced Raman spectroscopy *Adv. Mater.* **29** 1603601
[30] Campos-Delgado J, Cançado L G, Achete C A, Jorio A and Raskin J-P 2013 Raman scattering study of the phonon dispersion in twisted bi-layer graphene *Nano Res.* **6** 269–74
[31] Carozo V, Almedia C M, Ferreira E H M, Cançado L G, Achete C A and Jorio A 2011 Raman signature of graphene superlattices *Nano Lett.* **11** 4527–34
[32] Chan -C-C, Chung W-L and Woon W-Y 2018 Nucleation and growth kinetics of multi-layered graphene on copper substrate *Carbon* **135** 118–24
[33] Wang Y-H, Hong Y-Z, Chang L-Y, Chen C-H and Woon W-Y 2018 Structural reconstruction of reduced graphene *J. Phys. Chem.* C **122** 15876
[34] Cherian C T, Giustiniano F, Martin-Fernandez I, Andersen H, Balakrishnan J and Özyilmaz B 2015 "Bubble-free" electrochemical delamination of CVD graphene films *Small* **11** 189–94
[35] Dong J, Geng D, Liu F and Ding F 2019 Formation of twinned graphene polycrystals *Angew. Chem.* **131** 7805
[36] Chen Y *et al* 2014 Raman mapping investigation of chemical vapor deposition-fabricated twisted bilayer graphene with irregular grains *Phys. Chem. Chem. Phys.* **16** 21682
[37] Zhang X, Xu Z, Yuan Q, Xin J and Ding F 2015 The favourable large misorientation angle grain boundaries in graphene *Nanoscale* **7** 20082
[38] Guo W, Wu B, Li Y, Wang L, Chen J, Chen B, Zhang Z, Peng L, Wang S and Liu Y 2015 Governing rule for dynamic formation of grain boundaries in grown graphene *ACS Nano* **9** 5792